Cell Reports
Physical Science

CellPress
OPEN ACCESS

Article

Ionic organic cage-encapsulated metal clusters for switchable catalysis

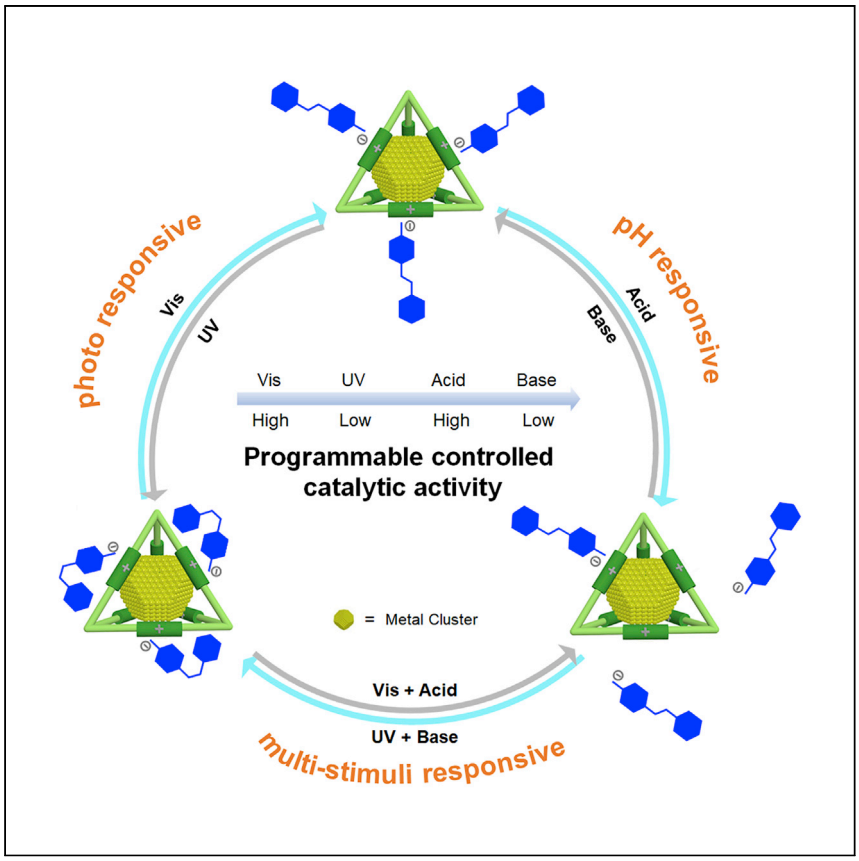

Systems in which catalytic activity can be modulated in response to external stimuli are desirable and challenging. Cao et al. present a switchable catalytic system by encapsulating metal clusters (MCs) inside cationic molecular cages (I-Cages) paired with dynamically tethered, responsive, and task-specific counteranions. This imparts a programmable gating effect for precise spatial and temporal control over chemical reactions.

Wei Cao, Junhao Zhou, Zdravko Kochovski, Han Miao, Zhiming Gao, Jian-Ke Sun, Jiayin Yuan

jiankesun@bit.edu.cn (J.-K.S.)
jiayin.yuan@mmk.su.se (J.Y.)

Highlights

Artificial switching catalysis encapsulates metal clusters in cationic molecular cages

Accessibility toward metal cluster surface is regulated by responsive counteranions

Precise spatial and temporal control over chemical reactions in a programmable way

Cao et al., Cell Reports Physical Science 2, 100546
September 22, 2021
https://doi.org/10.1016/j.xcrp.2021.100546

Cell Reports
Physical Science

CellPress
OPEN ACCESS

Article

Ionic organic cage-encapsulated metal clusters for switchable catalysis

Wei Cao,[1,2] Junhao Zhou,[1] Zdravko Kochovski,[3] Han Miao,[4] Zhiming Gao,[1] Jian-Ke Sun,[1,5,*] and Jiayin Yuan[2,*]

SUMMARY

The capability to build up stable, switchable catalysts for complex artificial systems that can mimic the responsiveness of biological systems to multiple triggers is highly desirable and challenging. Herein, we engineer such a system by physically locking catalytically active metal clusters (MCs) inside individual cationic molecular organic cages (I-Cages), where the responsive and task-specific counteranions of I-Cages impart MCs with a programmable gating effect. This allows for precise spatial and temporal control over chemical reactions by regulating accessibility of reagents to the MC sites. Following this strategy, we have successfully tailored catalytic activity of a series of model catalysis (e.g., methanolysis of ammonia borane, and the reduction of 4-nitroaniline) by employing light and pH stimuli, as well as their combination, for programmable-activity control.

INTRODUCTION

Artificial switchable catalysts, in which the catalytic activity can be modulated in response to external stimuli, have emerged as one of the most attractive themes recently because of their grand significance in mimicking specific and automatic, enzyme-driven reactions in nature.[1–6] Metal clusters (MCs) of high catalytic activity and selectivity are favorable for developing that switching catalysis.[7–9] Such MC-based catalytic systems are, to date, dominated by the surface-binding ligand approach including grafting functional capping agents and/or organic polymers onto MCs. In these cases, the external stimuli drives rearrangement of the ligand layer to substantially modulate the accessibility and subsequent catalytic activity of the underlying metal surface.[10,11] However, the ligand approach that relies on directly binding active sites of MCs suffers from the fact that the MC, as the core of this catalyst system. is labile and prone to size variation because of the altered metal-ligand binding strength upon external stimuli (temperature, pH, etc.), leading to cluster aggregation and the subsequent partial or total loss of activity.[12,13] In addition, this approach endures a trade-off, i.e., binding a high-energy, catalytically active surface by polar groups of ligands restricts the accessibility of reactants to these active sites during catalysis.[14–16] Therefore, improving both efficiency and stability of MC-based stimuli-responsive catalytic systems is highly desirable and challenging, in particular for complex artificial systems (e.g., mimicking the responsiveness of biological systems to multiple triggers) with advanced functions.[17–19]

An organic molecular cage is a class of multifunctional materials[20–30] that shows distinct advantages in confining MCs into its inner cavity for liquid-phase

[1]MOE Key Laboratory of Cluster Science, School of Chemistry and Chemical Engineering, Beijing Institute of Technology, 102488 Beijing, P. R. China

[2]Department of Materials and Environmental Chemistry, Stockholm University, 10691 Stockholm, Sweden

[3]Institute of Electrochemical Energy Storage, Helmholtz-Zentrum Berlin für Materialien und Energie, Hahn-Meitner-Platz 1, 14109 Berlin, Germany

[4]School of Materials Science and Engineering, Georgia Institute of Technology, Atlanta, GA 30332, USA

[5]Lead contact

*Correspondence: jiankesun@bit.edu.cn (J.-K.S.), jiayin.yuan@mmk.su.se (J.Y.)

https://doi.org/10.1016/j.xcrp.2021.100546

catalysis.[31–33] Its discrete micropore and molecular solubility in common solvents enables fairly soluble and processible MCs with more metal sites exposed to reagents for high activity than the ligand-based model.[34,35] In addition, the cage-confinement brings MCs with enhanced size stability, which can be sustained even in harsh chemical conditions, qualifying the cages as model catalytic systems.[36,37] In recent years, a series of MCs, including Au, Pd, Pt, Ag, and metal oxides, have been physically confined in organic cages for a broad range of catalytic reactions, including oxidation, dye degradation, and reduction reactions, among others.[38–43] Despite rapid progress in this area, few examples have been successful in achieving stimuli-responsive switching catalysis with this system.[44,45]

Herein, we design a stable MC-based "smart" catalytic system via an ionic molecular cage (I-Cage) approach, in which the cage cation locks the MC to avoid size variation and the associated anion brings the designable responsiveness that is then transferred to the MC. As such, instead of a conventional strategy to covalently or ionically bind stimuli-responsive ligands directly to the MC, here, we ionically associate them only to the I-Cage that physically encapsulates an MC in its core. The counter anions of I-Cage are easy to change and impart the MC core with programmable gating effects for precise spatial and temporal control over chemical reactions by regulating the accessibility to the metal sites. As a proof of concept, we successfully tailored the catalytic activity of a series of model catalyses (e.g., methanolysis of ammonia borane and reduction of 4-nitroaniline) by employing light and pH stimuli, as well as their combination for programmable activity control, which is highly desirable for an artificial catalyst to achieve on-demand catalytic activity for task-specific applications.[46–49]

RESULTS AND DISCUSSION

Synthesis and characterization of stimuli-responsive MC@I-Cages

Because of electrostatic repulsion, noble MCs locked inside cationic organic cages (denoted as MC@I-Cage) are well dispersed in solvents and are chemically paired with counter anions that are mobile and are associated with the I-Cage. Our idea was to introduce environmental-adaptive anions straightforward to the MC@I-Cage (Figure 1), so that the gating function is encoded into the chemical structure of the building units. The selected anions, e.g., azobenzoate (Azo) and octanoate (Oct) endowed MC@I-Cages-*X* (*X* = counter anion) with photo- and pH- responsive properties, respectively (Figure S1). The experiment started with synthesis of MC@I-Cage-Cl, in which MC was encapsulated into the parent I-Cage-Cl by wet chemical reduction of the corresponding metal salts, as reported previously.[45] Exchange of Cl^- with the above-mentioned specific counter anions generated MC@I-Cage-Azo and MC@I-Cage-Oct, respectively, with target gating functions (see supplemental information for synthetic details). The successful anion-exchange was confirmed by proton and carbon nuclear magnetic resonance (^{1}H-NMR and ^{13}C-NMR) spectroscopy (Figures S2–S9), which revealed a stoichiometric equivalent of 12 counter anions around one I-Cage (Figures S6–S8). The titration test of I-Cage-Cl with an aqueous $AgNO_3$ solution produced no precipitate, confirming the quantitative replacement of Cl^-. The size of the MCs of our interest, here Pt and Au, was determined by high-angle, annular, dark-field scanning transmission electron microscopy (HAADF-STEM) to be 0.54 $\pm$ 0.20 and 0.68 $\pm$ 0.20 nm, respectively (Figure 2), indicating that MCs remain encapsulated inside the I-Cage along with the anion-exchange process. X-ray photoelectron spectroscopy (XPS) measurements identified the expected existence of metallic Pt (binding

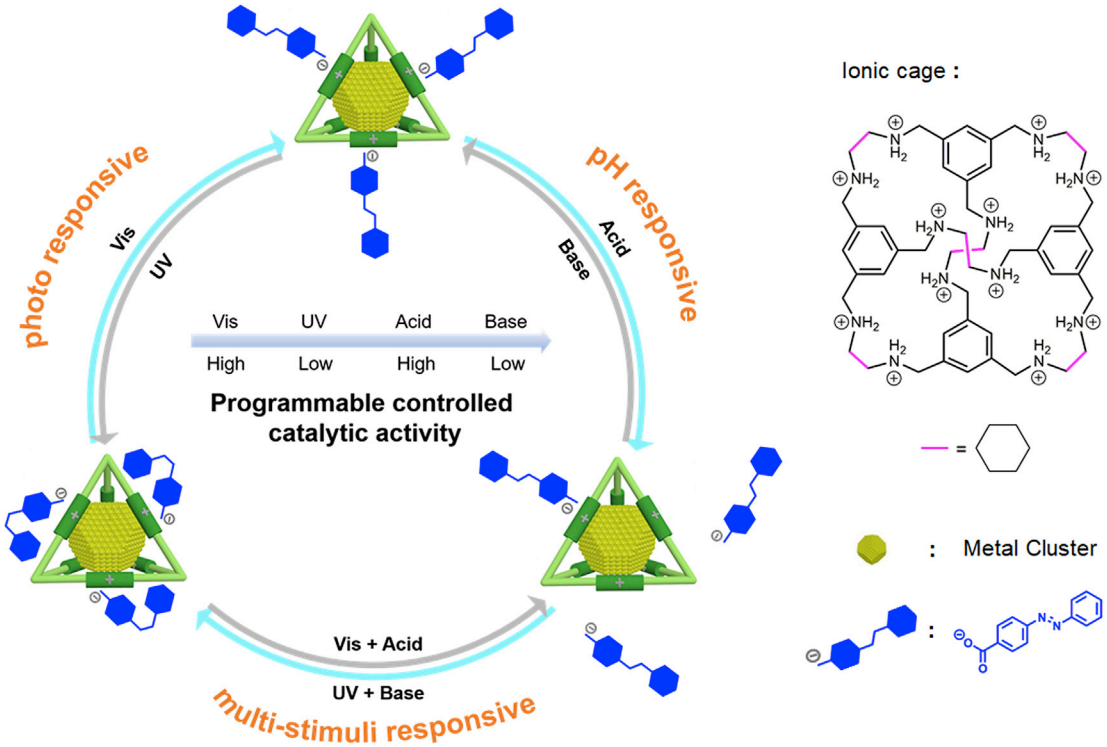

Figure 1. Schematic of stimuli-responsive MC@I-Cages

Schematic of photo-, pH- and multi-stimuli-responsive MC@I-Cages by responsive counteranions.

energy at 76.3 and 72.9 eV) (Figure S10A) and Au (binding energy at 88.7 and 84.2 eV) (Figure S10B)

Adjustable catalytic performance of Pt@I-Cage-Azo under photo-stimuli condition

As a model system, an Azo-cage was used to elucidate the stimuli-responsive process, which was mainly caused by the photoisomerization behavior of the azo moieties in the compound. Ultraviolet-visible (UV-vis) and ^{1}H-NMR spectroscopies were performed to study the photo-responsive process. Figure 3B displays the absorption spectra of Azo-cage in methanol solution (~0.01 mM) after continuous UV light irradiation. The absorbance at ~322 nm (assigned to the bonding-antibonding orbital [π-π*] transition of the *trans*-Azo moiety) decreases remarkably in intensity, whereas a slight increase of the band at ~430 nm appeared (assigned to the n-π* transition of the *cis*-Azo moiety). The photo-stationary state of the Azo-cage can be achieved after 5 min of irradiation, and the proportion of *trans*-Azo in the I-Cage-Azo varied from 85% to 30% (Table S1), as estimated by UV-Vis spectroscopy. Such a process is reversible upon irradiation with the visible light (Figure 3B, inset). The current system is robust and proven by at least six cycles (Figure 3C). In addition, the photoisomerization behavior of the Azo-cage was evaluated by ^{1}H NMR spectroscopy (Figures 3D, S11, and S12), along with a similar conversion ratio to that of UV-Vis spectral analysis.

After proving the photo-responsive properties of Azo-cage, the adjustable catalytic performance of Pt@I-Cage-Azo was investigated under the photo-stimuli condition using methanolysis reaction of ammonia borane (AB) as a model of catalysis (Scheme S1). Figure 3E showed the time course for hydrogen generation from the

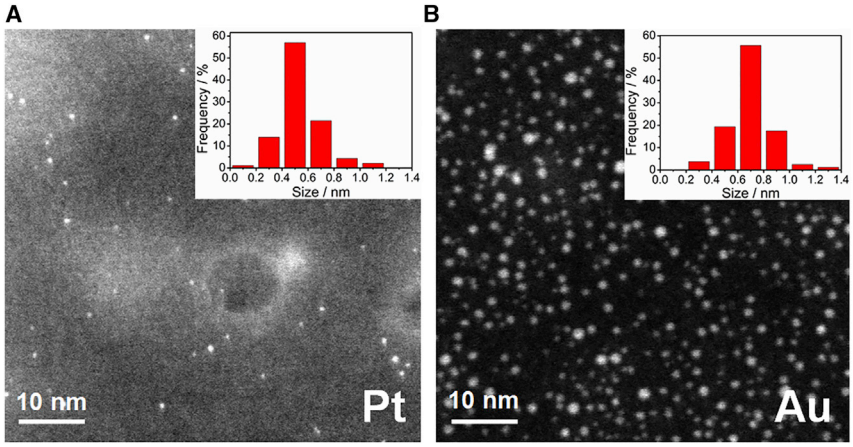

Figure 2. HAADF-STEM characterization of MC@I-Cages

(A) HAADF-STEM images and the size distribution histograms (in inset) of Pt@I-Cage-Azo.

(B) HAADF-STEM images and the size distribution histograms (in the inset) of Au@I-Cage-Oct.

Note that the cage itself is invisible; thus, the size obtained here stands only for the metallic core.

methanolysis of AB in the presence of Pt@I-Cage-Azo. Under Vis-irradiation, the reaction was completed in 6 min, with a turnover frequency (TOF) of 83 min^{-1} (Pt/AB = 0.006), whereas, under UV-irradiation, the reaction was completed in 16 min, with a TOF of 31 min^{-1}. These results indicate that the *trans* form of Azo moieties in the cage was more favorable to boost the catalytic activity. Moreover, the Pt@I-Cage-Cl did not show any activity change upon light-irradiation (Figure S13), indicative of a dominant role for the photoactive counteranion in modulating catalytic activity. To highlight the controllable catalytic activity of Pt@I-Cage-Azo, the reaction was conducted under alternating irradiation of UV and Vis light. As shown in Figure 3F, the repeated "fast/slow" cycle can proceed until the AB was completely consumed. Graphic representation for the transformation between *trans* and *cis* forms of Azo moieties in Pt@I-Cage-Azo was shown in Figure 3G.

To pinpoint the effect of a configurational change on the mechanism of switching catalysis, cryogenic electron microscopy (cryo-EM) analysis of samples before and after stimuli treatment was performed. An increase in the average size of Pt@I-Cage-Azo from 3.7 $\pm$ 0.40 to 4.4 $\pm$ 0.40 nm after Vis stimuli was observed (Figure S14), whereas the size of the MC as core according to HAADF-STEM measurements (Figure S15) is maintained. This outcome suggests that such size increase observed in cryo-EM after external stimuli treatment should be reasonably attributed to the configurational change of azo anion, which in turn alters the affinity between the azo anion and the cationic cage. Since the association of the counterions to the cages should be dynamic in solution, ^{1}H DOSY NMR was performed to compare the interaction between Azo anions and Pt@Cage under different conditions (Figures S16 and S17). The result clarifies that Azo anions diffuse faster after Vis irradiation ($D = 4.23 \times 10^{-6}$ cm^2 s^{-1}) than that after UV irradiation ($D = 3.49 \times 10^{-6}$ cm^2 s^{-1}), indicating the stronger interaction between Azo anions and Pt@Cage under UV condition. Because the ^{1}H diffusion-ordered spectroscopy (DOSY) NMR experiment measures the average dimension of the structures of the isomers, which sums over all directions and could be very comparable, such variation in the diffusion coefficient (21%) in the current system is large enough to reveal the different bind affinity of Azo containing isomers to a specific substance, which is also consistent with the variation in Azo isomers reported in the literature.[50] Dynamic light

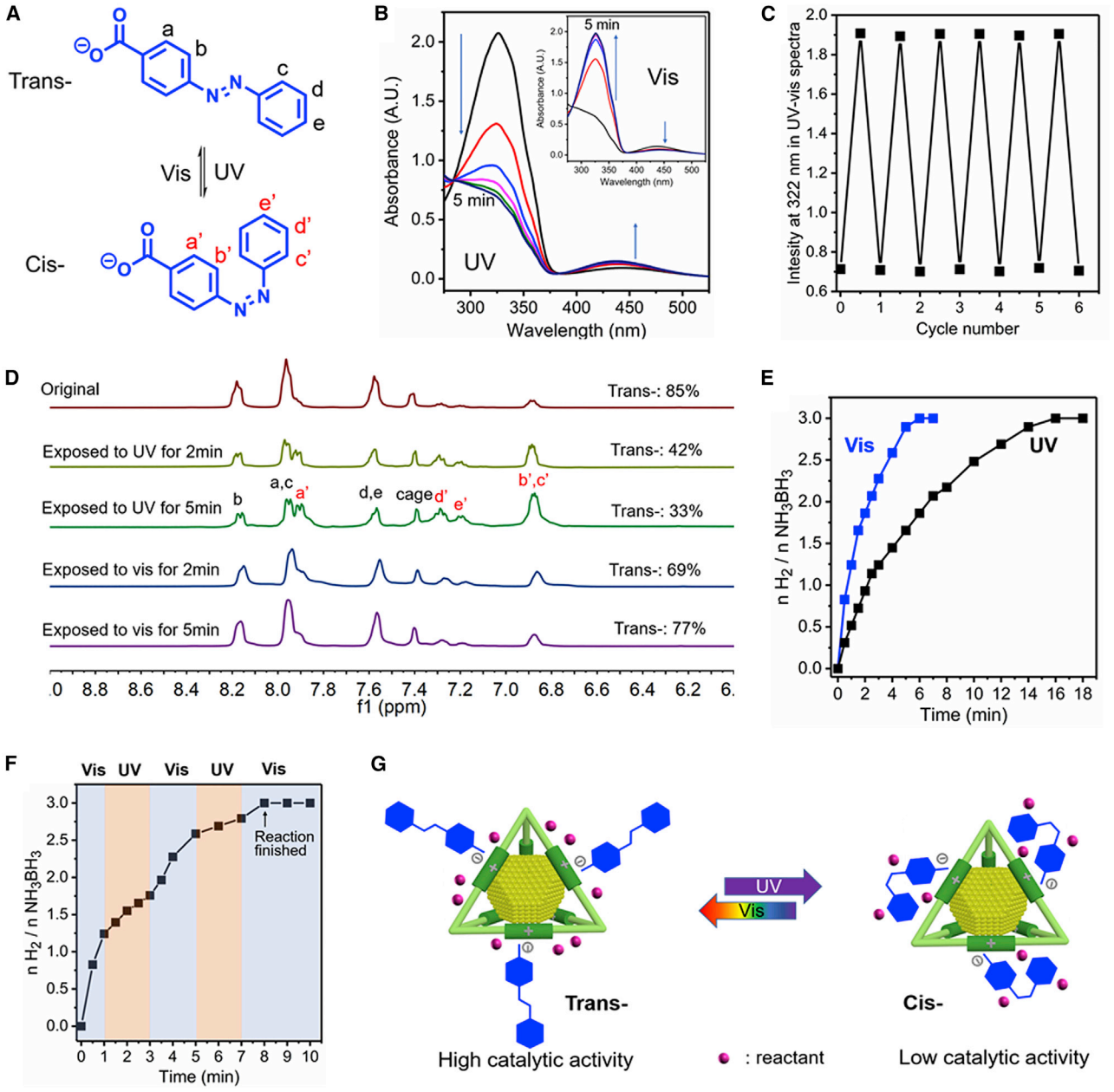

Figure 3. Photo-responsive catalytic performance of Pt@I-Cage-Azo

(A) *Trans* and *cis* states of the Azo anion. The positions of the hydrogen atoms are labeled alphabetically.

(B) Time-dependent UV-Vis spectra of the I-Cage-Azo in CD_3OD at 298 K, using UV and Vis (inset) irradiation.

(C) The changes of the absorption band of azo molecule at 322 nm upon alternating irradiation by UV and visible light.

(D) Time-dependent 400 MHz ^1H NMR spectra of I-Cage-Azo in CD_3OD at 298 K, using UV and Vis-irradiation.

(E) Time-course plot of hydrogen generation from methanolysis of ammonia borane (AB) in the presence of the Pt@I-Cage-Azo catalyst under irradiation of Vis (blue line) and UV light (black line) at 298 K.

(F) Controlling the hydrogen generation rate from AB methanolysis by altering Vis and UV irradiation.

(G) Graphic representation for the photo-responsive *trans*/*cis* conversion in Pt@I-Cage-Azo. Under Vis-irradiation the Azo moieties surrounding the cages mainly display the *trans* conformation (left), thus rendering additional accessible metal sites for the substrate to achieve high catalytic activity, whereas, under UV irradiation, the Azo moieties mainly display *cis* conformation (right), thus blocking additional metal sites from being accessed by the substrate, rendering the Pt@I-Cage-Azo with lower catalytic activity.

scattering (DLS) measurements showed an increase in the average size (hydrodynamic diameter) of Pt@I-Cage-Azo from 3.5 to 4.5 nm after Vis stimuli (Figures S18 and S19), which is consistent with the cryo-EM results (Figure S14). Next, the relative affinities of both *cis*- and *trans*-Azo for Pt@Cage were determined by means of a competition test with a fluorescent probe 8-anilino-1-naphthalenesulfonic acid (ANS) (Figure S20A), which was introduced into Pt@I-Cage-ANS by anion exchange with Cl^-. Note that ANS is barely fluorescent in pure water and is strongly fluorescent in contact with hydrophobic moieties (Figure S21[51]). In this test, *cis*-Azo and *trans*-Azo (Figure S22) were titrated separately to a HPEPES buffer (4-(2-hydroxyethyl)-1-piperazineethanesulfonic acid; 10 mM; pH, 7.0) aqueous solution of Pt@I-Cage-ANS (1 μM) (Figures S20B and S21). At that concentration, Pt@I-Cage-ANS had strong emissions because ANS can bind I-Cage through hydrophobic interactions to significantly enhance the fluorescence, as shown in Figure S21. The addition of increasing amounts of Azo anions resulted in the displacement of ANS in Pt@I-Cage-ANS by an anion-exchange reaction, which could be detected by a decrease in fluorescence intensity. The resulting displacement curves clearly showed that *cis*-Azo has a higher affinity (~1.6 times) to I-Cage than that of *trans*-Azo (Figure S20). Similar competition experiments with the fluorescent probe to reveal the affinity of *cis*- and *trans*-Azo for nanoparticles were previously reported in a Au cluster passivated by a monolayer of a surfactant system.[36–43] We also use molecular dynamics (MD) simulation to reveal that *cis*-Azo has a higher affinity to I-Cage because of the greater interaction energy (Figures S46 and S48A). It is reasonable that the less affinity of *trans*-Azo to the cage will provide a better accessibility window for substrates to contact metal sites (Figure 3G). Such a hypothesis was further demonstrated theoretically by analyzing the effects of a configuration change for Azo on the spatial arrangement around I-Cage via MD simulation (Videos S1 and S2). The less-sterical hindrance of *trans*-Azo around the I-Cage was then revealed by an averaged noncovalent interaction (NCI) analysis[52] of Pt@I-Cage-Azo in the corresponding configuration (Figure 4).

Adjustable catalytic performance of Au@I-Cage-Oct under pH-stimuli condition

Such switching catalytic behavior can be generalized and expanded to alternative stimuli, e.g., the pH for Au@I-Cage-Oct (Figure 5). The pH-stimuli-controlled catalytic activity of Au@I-Cage-Oct was studied using a model reaction: the reduction of 4-nitroaniline to 4-phenylenediamine by $NaBH_4$ (Scheme S2). Figure 5A displays a plot of $-\ln(C_t/C_0)$ versus time, in which a pseudo-first-order rate constant was determined. When catalyzed by the as-prepared Au@I-Cage-Oct, the reduction of 4-nitroaniline was completed in 27 min (Figure S23), with a reaction rate constant (k) of 0.155 min^{-1}. When treated by 1 molar equivalent H_2SO_4 (red dots) to protonate the octylcarboxylate anion (~99% protonation according to pK*a*), the reaction was completed in 8 min (Figure S24), along with a reaction rate constant of 0.518 min^{-1}, which is much faster than the pristine Au@I-Cage-Oct. Alternatively, when H_2SO_4 was replaced with HCl to protonate the octylcarboxylate anion, a similar result was observed (Figure S25). Note: as a control experiment, before and after adding 1 equivalent (eq.) of H_2SO_4 (molar ratio of n_{proton}/n_{Cl} = 1:1), the parent Au@I-Cage-Cl catalyst exhibited no activity difference toward the reduction of 4-nitroaniline (Figures S26–S28). The pH-controlled catalytic activity of Au@I-Cage-Oct was reversible by adding a base ($Ba(OH)_2$) into the above solution to simultaneously neutralize the HOct and remove the SO_4^{2-} anion in solution. (The final pH value of the solution was 7.67, in a good agreement with the original one at ~7.62) (Figure S29). We speculate that the pH stimuli can alter the electrostatic interaction strength between the cationic I-Cage and the counter anions, which influence

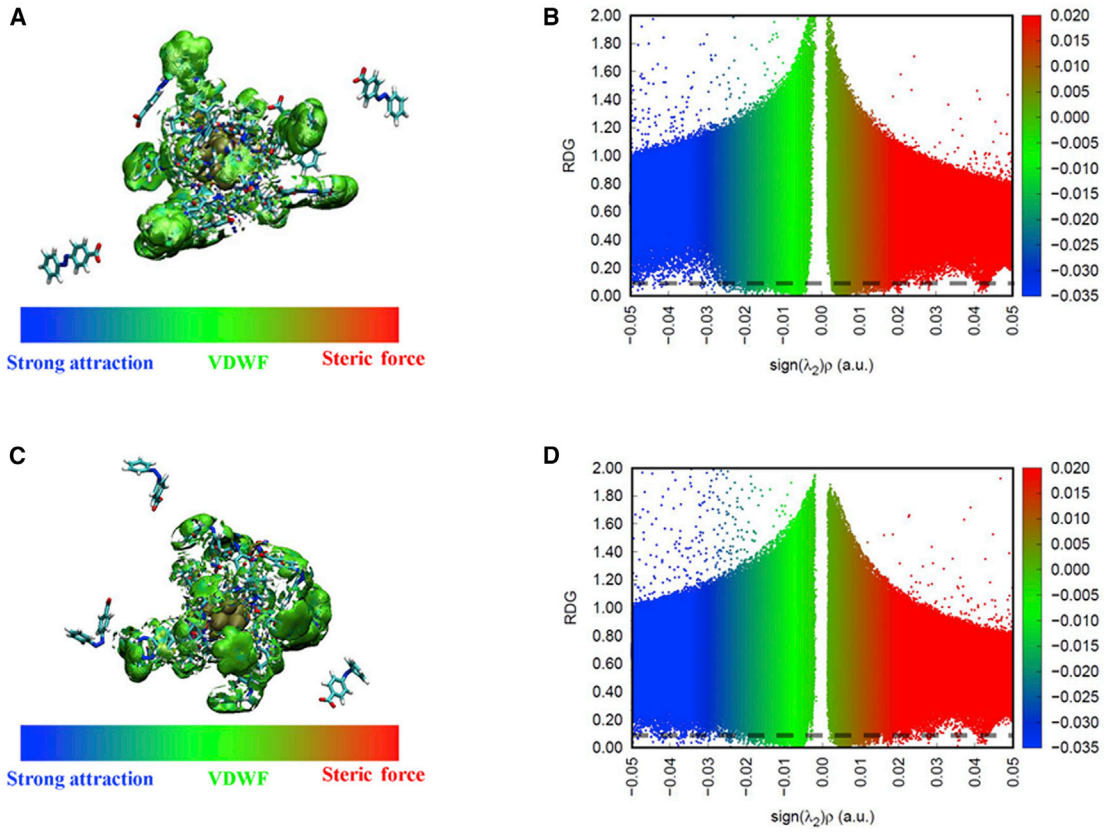

Figure 4. Color-filled reduced-density gradient isosurface and scatterplots depicting the average noncovalent interaction regions for the Pt@I-Cage-Azo

(A–D) Color-filled reduced-density gradient (RDG) isosurface and scatterplots depicting the average noncovalent interaction (NCI) regions for (A and B) Pt@I-Cage-Azo-*trans* and (C and D) Pt@I-Cage-Azo-*cis*. In the isosurface graphs, the blue-green-red color range, as shown in the color bar, was used to describe the value of sign $(\lambda_2)\rho$ from −0.03 to 0.02 a.u. Blue represents strong attractive interactions; green, van der Waals interactions; and red, the steric effect. The dotted triangle indicatess the cage molecule scaffolding for clarity. On the scatter diagrams, the more scatter points distributed on the line of 0.1 a.u. RDG, the stronger the corresponding interactions are.

the contact efficiency between the metal site and the substrate (Figure 5B). Such a hypothesis was supported by the cryo-EM measurements. A larger diameter was evidenced once after reducing the strength of the electrostatic interaction (3.4 ± 0.40 nm for pristine Au@I-Cage-Oct and 4.5 ± 0.40 nm after acid stimuli) (Figures S30 and S31), whereas the size of MCs were kept constant in the HADDF-STEM analyses (Figure S32). ^{1}H DOSY NMR of the Au@I-Cage-Oct before and after acid stimuli (Figure S33 and S34) was also performed. The result shows that the Oct anions diffused faster after acid stimuli of Au@I-Cage-Oct ($D = 6.46 \times 10^{-6}$ cm^2 s^{-1}) than they did in the original ($D = 4.35 \times 10^{-6}$ cm^2 s^{-1}), indicating that the interaction between the Oct anions and the Au@Cage became weaker after acid stimuli of Au@I-Cage-Oct. The DLS measurements showed an increase in the average size of the Au@I-Cage-Oct from 3.2 to 4.5 nm after acid stimuli (Figures S35 and S36), which is consistent with the cryo-EM results (Figures S30 and S31). The MD simulation revealed that protonation of Oct leads to a weaker affinity to the I-Cage when compared with that of the original (Figures S47 and S48B). Furthermore, the optimized spatial arrangement and steric effect of the anions around the I-Cage were identified by theoretical calculations (Figure S49; Note S1; Videos S3 and S4). The decrease in the electrostatic attraction between the I-Cage and the counter anions will expose more metal sites to the substrate, which enhances catalytic activity.

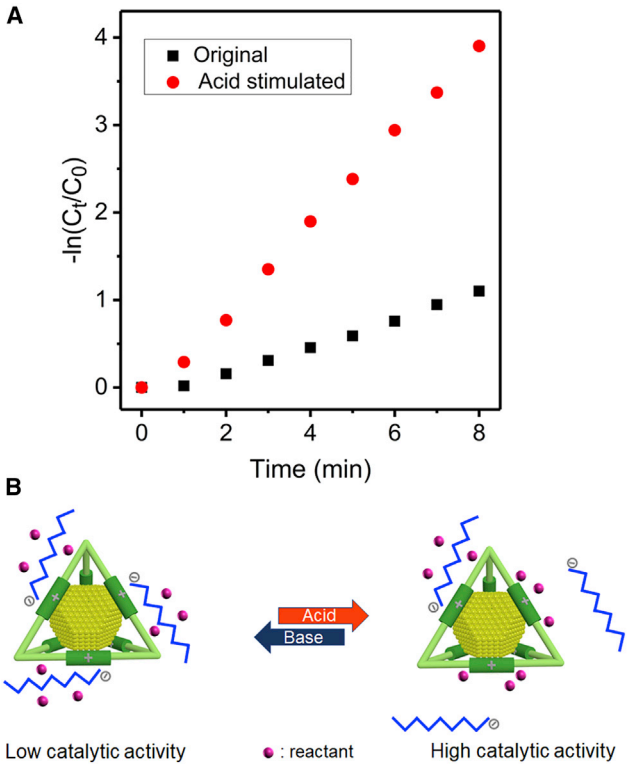

Figure 5. pH-responsive catalytic performance of Au@I-Cage-Oct

(A) Kinetic plot of $-\ln(C_t/C_0)$ versus time for the reduction of 4-nitroaniline to 4-phenylenediamine catalyzed by Au@I-Cage-Oct and mediated by pH stimuli (black dot, original catalyst; red dot, after adding acid).

(B) Graphic representation of the spatial arrangement of counteranions via pH stimuli in Au@I-Cage-Oct.

Tandem multi-stimuli-responsive catalysis

After success in single-stimulus-responsive catalysis, the tandem multi-stimuli-responsive catalysis was carried out by exerting various external stimuli simultaneously. Because the carboxylate group containing the Azo anion is both pH and light active, we conducted systematic control over the catalytic reaction in a programmable manner. Au@I-Cage-Azo was chosen to catalyze the model catalysis of the reduction of 4-nitroaniline. Figure 6A displays plots of $-\ln(C_t/C_0)$ versus time for the reaction catalyzed by Au@I-Cage-Azo under varied stimuli conditions (Figures S37–S44). The greatest catalytic activity for Au@I-Cage-Azo was achieved by simultaneous Vis-irradiation and acid addition (black square), whereas the least was from simultaneous UV irradiation and base addition (the violet inverted triangle). (The Au cluster itself is inert to the change of light irradiation, as verified in Figure S45). The corresponding *k* values under different stimuli are listed in Table S2. Such altered behavior activity is associated with the configuration and spatial arrangement of Au@I-Cage-Azo by various dual stimuli. Based on the above-mentioned stimuli-responsive behavior, the catalytic activity of Au@I-Cage-Azo toward 4-nitroaniline reduction was further programmably controlled by light and pH stimuli, in sequence, at different periods. As shown in Figure 6B, at the beginning, the reaction was irradiated by Vis light for 2 min and showed a normal reaction rate (monitored by the changing concentration of 4-nitroaniline via UV-vis spectra); thereafter, the reaction was irradiated by UV light for 2 min, and the reaction was observed to slow down. Afterward, by adding H_2SO_4 (1 eq. to the catalyst [cat.]),

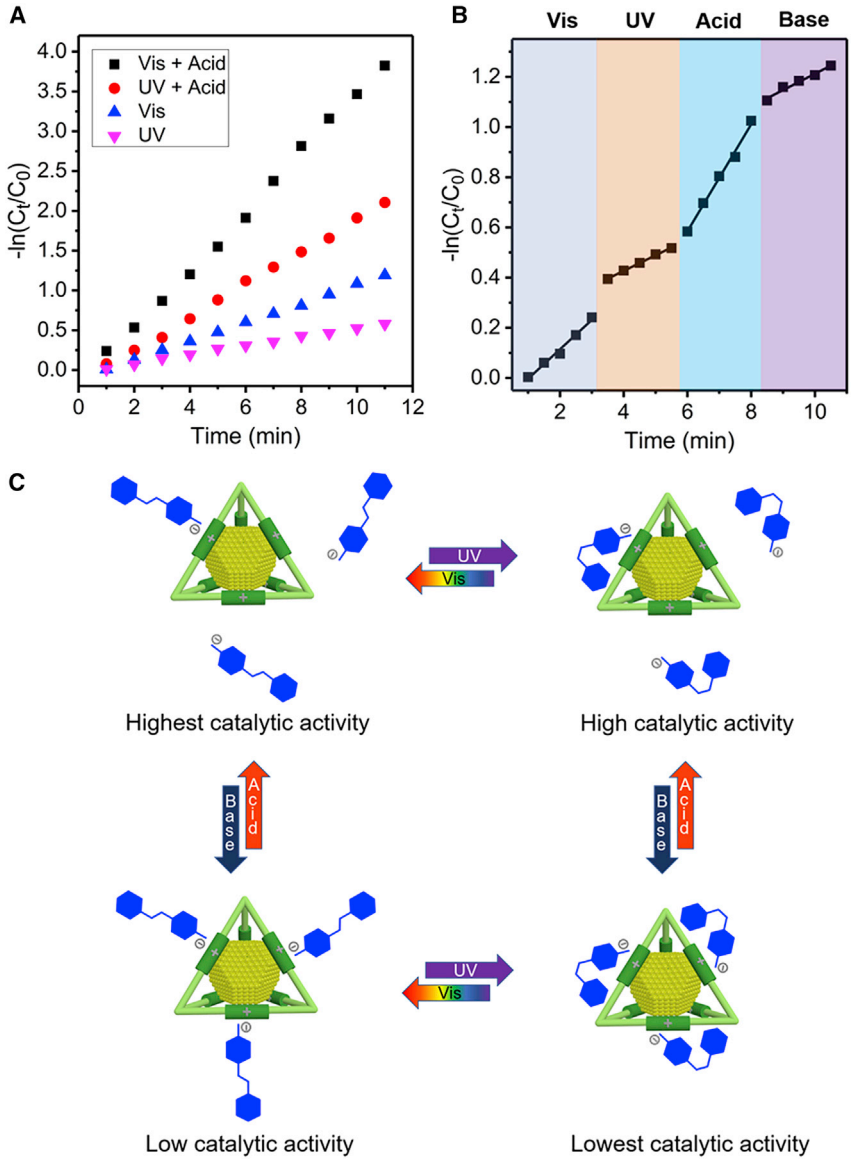

Figure 6. Tandem multi-stimuli responsive catalytic performance of Au@I-Cage-Azo

(A) Plots of $-\ln(C_t/C_0)$ versus time for the reaction catalyzed by Au@I-Cage-Azo under various stimuli conditions. Black squares represent Vis/acid conditions; red cycles, UV/acid conditions; blue triangles, Vis conditions; and violet inverted triangles, UV condition.

(B) Programmable control over the catalytic activity by light and pH stimuli in sequence at different periods.

(C) Graphic representation of the dual-stimuli-responsive behavior of the Azo anion around the I-Cage.

the reaction accelerated, and then, decelerated again, by adding $Ba(OH)_2$ (1 eq. to the cat.). Overall, the on-demand catalytic activity can be achieved by a combination of specific external stimuli in sequence.

In conclusion, we have established a switching catalysis system by encapsulating MC inside cationic I-Cages paired with stimuli-responsive anions. The original catalyst exhibits moderate catalytic activity toward the liquid phase catalytic reaction, e.g., the methanolysis reaction of AB (TOF: 31 min^{-1}), and reduction of 4-nitroaniline

(rate constant k of 0.155 min^{-1}), and its catalytic properties can be manipulated via external stimuli, such as light and pH, by reconfiguration/rearrangement of the counter-anions around the I-Cage with several-fold enhancement (methanolysis reaction of AB, TOF: 88 min^{-1}, reduction of 4-nitroaniline, k = 0.518 min^{-1}). Moreover, programmable control over the activity by a combination of different stimuli in a sequential manner is demonstrated. Such a catalytic system is valuable because of some of the attractive features of the biological counterparts and may inspire researchers to extend the concepts of programmable catalysis in future biomimetic catalysts.

EXPERIMENTAL PROCEDURES

Resource availability

Lead contact

Further information and requests for resources and materials should be directed to, and will be fulfilled by, the lead contact Jian-Ke Sun (jiankesun@bit.edu.cn).

Materials availability

No new unique reagents were generated in this study.

Data and code availability

The authors declare that all of the data supporting the findings of this study are available within the article and supplemental information. Additional information is available from the lead contact upon reasonable request.

SUPPLEMENTAL INFORMATION

Supplemental information can be found online at https://doi.org/10.1016/j.xcrp.2021.100546.

ACKNOWLEDGMENTS

J.-K.S. is grateful for the financial support from the National Natural Science Foundation of China (grant nos. 22071008 and 52003029), the Fundamental Research Funds for the Central Universities, and a start-up grant from the Beijing Institute of Technology (3100011181910). The technical support from the staff at the Analysis & Testing Center, Beijing Institute of Technology is also appreciated. J.Y. is grateful for financial support from the European Research Council (ERC; starting grant NAPOLI-639720), the Swedish Research Council (grant 2018-05351), Dozentenpreis 15126 from Verband der Chemischen Industrie (VCI) in Germany, the Wallenberg Academy Fellow program (grant KAW 2017.0166) in Sweden, and the Stockholm University Strategic Fund SU FV-2.1.1-005. Z.K. thanks the Joint Laboratory for Structural Research at the Integrative Research Institute for the Sciences (IRIS Adlershof, Berlin) for Cryo-EM imaging.

AUTHOR CONTRIBUTIONS

W.C. conceived the idea, conducted most of the experiments, and analyzed the data. J.Z. contributed to the simulation. Z.K. contributed to cryo-EM imaging. H.M. contributed to TEM, XPS, and DOSY NMR characterization. Z.G. assisted in data analysis. J.-K.S. and J.Y. directed the project and conceived the idea. W.C., J.-K.S., and J.Y. wrote the manuscript with input from all of the authors. All of the authors contributed to the editing of the manuscript and discussed the results.

DECLARATION OF INTERESTS

The authors declare no competing interests

Received: May 20, 2021
Revised: July 7, 2021
Accepted: July 28, 2021
Published: August 23, 2021

REFERENCES

1. Blanco, V., Leigh, D.A., and Marcos, V. (2015). Artificial switchable catalysts. Chem. Soc. Rev. *44*, 5341–5370.

2. Lüning, U. (2012). Switchable catalysis. Angew. Chem. Int. Ed. Engl. *51*, 8163–8165.

3. Semwal, S., and Choudhury, J. (2017). Switch in catalyst state: single bifunctional bi-state catalyst for two different reactions. Angew. Chem. Int. Ed. Engl. *56*, 5556–5560.

4. Stoll, R.S., and Hecht, S. (2010). Artificial light-gated catalyst systems. Angew. Chem. Int. Ed. Engl. *49*, 5054–5075.

5. Wiester, M.J., Ulmann, P.A., and Mirkin, C.A. (2011). Enzyme mimics based upon supramolecular coordination chemistry. Angew. Chem. Int. Ed. Engl. *50*, 114–137.

6. Wang, J., and Feringa, B.L. (2011). Dynamic control of chiral space in a catalytic asymmetric reaction using a molecular motor. Science *331*, 1429–1432.

7. Vassalini, I., and Alessandri, I. (2018). Switchable stimuli-responsive heterogeneous catalysis. Catalysts *8*, 569.

8. Nasaruddin, R.R., Chen, T., Yan, N., and Xie, J. (2018). Roles of thiolate ligands in the synthesis, properties and catalytic application of gold nanoclusters. Coord. Chem. Rev. *368*, 60–79.

9. Zaupa, G., Mora, C., Bonomi, R., Prins, L.J., and Scrimin, P. (2011). Catalytic self-assembled monolayers on Au nanoparticles: the source of catalysis of a transphosphorylation reaction. Chemistry *17*, 4879–4889.

10. Szewczyk, M., Sobczak, G., and Sashuk, V. (2018). Photoswitchable catalysis by a small swinging molecule confined on the surface of a colloidal particle. ACS Catal. *8*, 2810–2814.

11. Neri, S., Garcia Martin, S., Pezzato, C., and Prins, L.J. (2017). Photoswitchable catalysis by a nanozyme mediated by a light-sensitive cofactor. J. Am. Chem. Soc. *139*, 1794–1797.

12. Chevrier, D.M., Raich, L., Rovira, C., Das, A., Luo, Z., Yao, Q., Chatt, A., Xie, J., Jin, R., Akola, J., and Zhang, P. (2018). Molecular-scale ligand effects in small gold-thiolate nanoclusters. J. Am. Chem. Soc. *140*, 15430–15436.

13. Wang, Y., Wan, X.K., Ren, L., Su, H., Li, G., Malola, S., Lin, S., Tang, Z., Häkkinen, H., Teo, B.K., et al. (2016). Atomically precise alkynyl-protected metal nanoclusters as a model catalyst: observation of promoting effect of surface ligands on catalysis by metal nanoparticles. J. Am. Chem. Soc. *138*, 3278–3281.

14. Sun, J.K., Kochovski, Z., Zhang, W.Y., Kirmse, H., Lu, Y., Antonietti, M., and Yuan, J. (2017). General synthetic route toward highly dispersed metal clusters enabled by poly(ionic liquid)s. J. Am. Chem. Soc. *139*, 8971–8976.

15. Du, Y., Sheng, H., Astruc, D., and Zhu, M. (2020). Atomically precise noble metal nanoclusters as efficient catalysts: a bridge between structure and properties. Chem. Rev. *120*, 526–622.

16. Zhao, Y., Zhuang, S., Liao, L., Wang, C., Xia, N., Gan, Z., Gu, W., Li, J., Deng, H., and Wu, Z. (2020). A dual purpose strategy to endow gold nanoclusters with both catalysis activity and water solubility. J. Am. Chem. Soc. *142*, 973–977.

17. Marchetti, L., and Levine, M. (2011). Biomimetic catalysis. ACS Catal. *9*, 1090–1118.

18. Ferguson, C.T.J., Huber, N., Landfester, K., and Zhang, K.A.I. (2019). Dual-responsive photocatalytic polymer nanogels. Angew. Chem. Int. Ed. Engl. *58*, 10567–10571.

19. Grzybowski, B.A., and Huck, W.T.S. (2016). The nanotechnology of life-inspired systems. Nat. Nanotechnol. *11*, 585–592.

20. Hasell, T., and Cooper, A.I. (2016). Porous organic cages: soluble, modular and molecular pores. Nat. Rev. Mater. *1*, 16053.

21. Mukhopadhyay, R.D., Kim, Y., Koo, J., and Kim, K. (2018). Porphyrin boxes. Acc. Chem. Res. *51*, 2730–2738.

22. Zhang, G., Presly, O., White, F., Oppel, I.M., and Mastalerz, M. (2014). A permanent mesoporous organic cage with an exceptionally high surface area. Angew. Chem. Int. Ed. Engl. *53*, 1516–1520.

23. Lavendomme, R., Ronson, T.K., and Nitschke, J.R. (2019). Metal and organic templates together control the size of covalent macrocycles and cages. J. Am. Chem. Soc. *141*, 12147–12158.

24. Beuerle, F., and Gole, B. (2018). Covalent organic frameworks and cage compounds: design and applications of polymeric and discrete organic scaffolds. Angew. Chem. Int. Ed. Engl. *57*, 4850–4878.

25. Dale, E.J., Vermeulen, N.A., Thomas, A.A., Barnes, J.C., Juríček, M., Blackburn, A.K., Strutt, N.L., Sarjeant, A.A., Stern, C.L., Denmark, S.E., and Stoddart, J.F. (2014). ExCage. J. Am. Chem. Soc. *136*, 10669–10682.

26. Yan, X., Cook, T.R., Wang, P., Huang, F., and Stang, P.J. (2015). Highly emissive platinum(II) metallacages. Nat. Chem. *7*, 342–348.

27. Cai, L.X., Li, S.C., Yan, D.N., Zhou, L.P., Guo, F., and Sun, Q.F. (2018). Water-soluble redox-active cage hosting polyoxometalates for selective desulfurization catalysis. J. Am. Chem. Soc. *140*, 4869–4876.

28. Grommet, A.B., Feller, M., and Klajn, R. (2020). Chemical reactivity under nanoconfinement. Nat. Nanotechnol. *15*, 256–271.

29. Jie, K., Onishi, N., Schott, J.A., Popovs, I., Jiang, D.E., Mahurin, S., and Dai, S. (2020). Transforming porous organic cages into porous ionic liquids via a supramolecular complexation strategy. Angew. Chem. Int. Ed. Engl. *59*, 2268–2272.

30. Hua, M., Wang, S., Gong, Y., Wei, J., Yang, Z., and Sun, J.K. (2021). Hierarchically porous organic cages. Angew. Chem. Int. Ed. Engl. *60*, 12490–12497.

31. Yang, X., Sun, J.K., Kitta, M., Pang, H., and Xu, Q. (2018). Encapsulating highly catalytically active metal nanoclusters inside porous organic cages. Nat. Catal. *1*, 214–220.

32. Yang, X., and Xu, Q. (2020). Encapsulating metal nanocatalysts within porous organic hosts. Trends Chem. *2*, 214–226.

33. Yang, X., Chen, L., Liu, H., Kurihara, T., Horike, S., and Xu, Q. (2021). Encapsulating ultrastable metal nanoparticles within reticular Schiff base nanospaces for enhanced catalytic performance. cell reports physical. Science *2*, 100289.

34. Sun, J.K., Zhan, W.W., Akita, T., and Xu, Q. (2015). Toward homogenization of heterogeneous metal nanoparticle catalysts with enhanced catalytic performance: soluble porous organic cage as a stabilizer and homogenizer. J. Am. Chem. Soc. *137*, 7063–7066.

35. Zhang, Y., Xiong, Y., Ge, J., Lin, R., Chen, C., Peng, Q., Wang, D., and Li, Y. (2018). Porous organic cage stabilised palladium nanoparticles: efficient heterogeneous catalysts for carbonylation reaction of aryl halides. Chem. Commun. (Camb.) *54*, 2796–2799.

36. Inomata, T., and Konishi, K. (2003). Gold nanocluster confined within a cage: template-directed formation of a hexaporphyrin cage and its confinement capability. Chem. Commun. (Camb.) (11), 1282–1283.

37. McCaffrey, R., Long, H., Jin, Y., Sanders, A., Park, W., and Zhang, W. (2014). Template synthesis of gold nanoparticles with an organic molecular cage. J. Am. Chem. Soc. *136*, 1782–1785.

38. Mondal, B., Acharyya, K., Howlader, P., and Mukherjee, P.S. (2016). Molecular cage impregnated palladium nanoparticles: efficient, additive-free heterogeneous catalysts for cyanation of aryl halides. J. Am. Chem. Soc. *138*, 1709–1716.

39. Jiang, S., Cox, H.J., Papaioannou, E.I., Tang, C., Liu, H., Murdoch, B.J., Gibson, E.K., Metcalfe, I.S., Evans, J.S.O., and Beaumont, S.K. (2019). Shape-persistent porous organic cage supported palladium nanoparticles as heterogeneous catalytic materials. Nanoscale *11*, 14929–14936.

40. Chen, G.J., Xin, W.L., Wang, J.S., Cheng, J.Y., and Dong, Y.B. (2019). Visible-light triggered selective reduction of nitroarenes to azo compounds catalysed by Ag@organic molecular cages. Chem. Commun. (Camb.) *55*, 3586–3589.

41. Sun, N., Wang, C., Wang, H., Yang, L., Jin, P., Zhang, W., and Jiang, J. (2019). Multifunctional tubular organic cage-supported ultrafine palladium nanoparticles for sequential catalysis. Angew. Chem. Int. Ed. Engl. *58*, 18011–18016.

42. Zhang, S.Y., Miao, H., Zhang, H.M., Zhou, J.H., Zhuang, Q., Zeng, Y.J., Gao, Z., Yuan, J., and Sun, J.K. (2020). Accelerating crystallization of open organic materials by poly(ionic liquid)s. Angew. Chem. Int. Ed. Engl. *59*, 22109–22116.

43. Gou, X.X., Liu, T., Wang, Y.Y., and Han, Y.F. (2020). Ultrastable and highly catalytically active n-heterocyclic-carbene-stabilized gold nanoparticles in confined spaces. Angew. Chem. Int. Ed. Engl. *59*, 16683–16689.

44. Cullen, W., Misuraca, M.C., Hunter, C.A., Williams, N.H., and Ward, M.D. (2016). Highly efficient catalysis of the Kemp elimination in the cavity of a cubic coordination cage. Nat. Chem. *8*, 231–236.

45. Zhang, S.Y., Kochovski, Z., Lee, H.C., Lu, Y., Zhang, H., Zhang, J., Sun, J.K., and Yuan, J. (2018). Ionic organic cage-encapsulating phase-transferable metal clusters. Chem. Sci. (Camb.) *10*, 1450–1456.

46. Wang, J., Yue, L., Li, Z., Zhang, J., Tian, H., and Willner, I. (2019). Active generation of nanoholes in DNA origami scaffolds for programmed catalysis in nanocavities. Nat. Commun. *10*, 4963.

47. Zhou, T.Y., Auer, B., Lee, S.J., and Telfer, S.G. (2019). Catalysts confined in programmed framework pores enable new transformations and tune reaction efficiency and selectivity. J. Am. Chem. Soc. *141*, 1577–1582.

48. Kassem, S., Lee, A.T.L., Leigh, D.A., Marcos, V., Palmer, L.I., and Pisano, S. (2017). Stereodivergent synthesis with a programmable molecular machine. Nature *549*, 374–378.

49. Craven, E.J., Latham, J., Shepherd, S.A., Khan, I., Diaz-Rodriguez, A., Greaney, M.F., and Micklefield, J. (2021). Programmable late-stage C−H bond functionalization enabled by integration of enzymes with chemocatalysis. Nat. Catal. *4*, 385–394.

50. Adam, A., Mehrparvar, S., and Haberhauer, G. (2019). An azobenzene container showing a definite folding - synthesis and structural investigation. Beilstein J. Org. Chem. *15*, 1534–1544.

51. Schönbrunn, E., Eschenburg, S., Luger, K., Kabsch, W., and Amrhein, N. (2000). Structural basis for the interaction of the fluorescence probe 8-anilino-1-naphthalene sulfonate (ANS) with the antibiotic target MurA. Proc. Natl. Acad. Sci. USA *97*, 6345–6349.

52. Wu, P., Chaudret, R., Hu, X., and Yang, W. (2013). Noncovalent interaction analysis in fluctuating environments. J. Chem. Theory Comput. *9*, 2226–2234.